Laki To Tambora

A study of ice cores

Thea Quistgaard

Master Thesis 2020/2021

Figure 1: J. M. W. Turner: *The Eruption of the Soufriere Mountains*

Darkness

I had a dream, which was not all a dream.
The bright sun was extinguish'd, and the stars
Did wander darkling in the eternal space,
Rayless, and pathless, and the icy earth
Swung blind and blackening in the moonless air;
Morn came and went—and came, and brought no day.

Lord Byron (1788–1824)

Acknowledgments

I would like to thank potatoes. They are great.

Abstract

Contents

List of Figures

List of Tables

Listings

Chapter 1

Introduction

This is an amazing introduction that shows that I know all the stuff that I have done in my thesis. I am clever clever clever.

Chapter 2

The theory of ice cores

2.1 Water Isotopes and δ-notation

A corner stone in ice core analysis, which helps lay the basis for paleo climate research, is through measurements of the isotopic composition of the water - or that of the encapsulated air in bubbles - which makes up the ice cores. Water isotopes are sensitive to temperature changes and can thus be used as a proxy for paleo temperature along with being used as dating parameters, since the annual cycles often are detectable in water isotope data.

δ notation and water isotopes

Water isotopic ratios, i.e. the ratio of the minority isotope, $H_2^{18}O$ or $H_2^{17}O(^2H_2O)$, compared to the majority isotope, $H_2^{16}O$ (^1H_2O), are used to report the quantities of isotopes in a sample relative to the ratio of a given reference water sample. This is commonly expressed in the δ-notation as:

$$\delta^i = \frac{^iR_{sample}}{^iR_{reference}} - 1 \tag{2.1}$$

where $^{18}R = \frac{n_{^{18}\mathrm{O}}}{n_{^{16}\mathrm{O}}}$, $^{2}R = \frac{n_{^{2}\mathrm{H}}}{n_{^{1}\mathrm{H}}}$ and $^{17}R = \frac{n_{^{17}\mathrm{O}}}{n_{^{16}\mathrm{O}}}$. Here n is the abundance of the given isotope.
Besides the isotopic quantities $\delta^{17}O$, $\delta^{18}O$ and $\delta^2H = \delta D$, both deuterium excess and $\Delta^{17}O$, known as ^{17}O excess, can be of interest. Deuterium excess is usually used as a measure of the kinetic fractionation processes, taking place in the water vapor formation of polar precipitation, giving an indicator of the conditions during precipitation formation, and thus giving a pointer to the source of the water vapor. Like deuterium excess ^{17}O is sensi-

tive to kinetic fractionation, but much less sensitive to equilibrium fractionation than both δD and δ^{18}O. Along with being nearly insensitive to temperature(REFERENCES), these robustness factors leads to ^{17}O being usable as an independent parameter to be used to reveal the ways of the complicated mixing effects of fractionation due to evaporation, transportation, formation and deposition.

2.2 Diffusion and Densification

Throughout the firn column the important processes of diffusion and densification takes places. Both processes need to be well understood and examined when analyzing ice core data, as diffusion and densification play a large role in thinning of annual layers due to compression of snow to ice and in washing out the measured signals through diffusion in the firn.

2.2.1 Densification

Densification is the process of compression of snow to ice. It plays an important role in the annual layer thickness in the data as snow will be compressed to a smaller volume under pressure from the firn column above until it reaches a solid ice state with a, almost, constant density.
Commonly three stages of densification are described in the firn column. The first stage is between the initial precipitated snow density and the 'critical density' at $0.55\frac{\mathrm{Mg}}{\mathrm{m}^3}$, the second stage is between critical density and the close-off density at $0.82 - 0.84\frac{\mathrm{Mg}}{\mathrm{m}^3}$, and the third stage is from close-off and all the way through the ice.
At the first stage the densification is mostly due to grain settling and packing and the densification rate is very rapid. At the second stage, the snow is close to isolating air bubbles. At the third stage, the dominating densification taking place is by the compression of air bubbles.
For these three stages it is of interest to develop a depth-density profile, which is dependent on snow accumulation rate and temperature. The focus is on developing an empirical model for the first and second stages of densification, as they are the most dramatic sections of the firn column considering densification and diffusion.
A number of different densification models have been developed(REFERENCES), and in this thesis will be presented the ones used for the analysis.

Herron Langway Empirical Model

Sorge's law(REFERENCES) assumes that the relation between snow density ρ and depth h is invariant with time, given a constant snow accumulation and temperature. Furthermore, annual layer thinning by plastic flow is ignored. Densification of firn, which can be described as the proportional change in air space, is linearly related to change in stress due to the weight of the overlying snow(REFERENCES):

$$\frac{d\rho}{\rho_i - \rho} = \text{const.}\, \rho\, dh \tag{2.2}$$

By integration, this implies a linear relation between $\ln\left[\frac{\rho}{\rho_i-\rho}\right]$ and h.

When considering real data, analysis shows that $\ln\left[\frac{\rho}{\rho_i-\rho}\right]$ vs h. plots have two linear segments(EXAMPLE), corresponding to the first and second stages of densification, with separation of segments at $\rho = 0.55$ and $\rho = 0.8$. These segments on the plots will yield two different slopes with slope constants:

$$C = \frac{d\ln\left[\frac{\rho}{\rho_i-\rho}\right]}{dh}, \rho < 0.55 \tag{2.3a}$$

$$C' = \frac{d\ln\left[\frac{\rho}{\rho_i-\rho}\right]}{dh}, 0.55 < \rho < 0.8 \tag{2.3b}$$

To find the densification rate, $\frac{d\rho}{dt}$, substitute $\frac{dh}{dt} = \frac{A}{\rho} \rightarrow dt = \frac{\rho}{A}dh$ and use the differentiation $\frac{\partial}{\partial t}\left[\ln\left[\frac{x(t)}{k-x(t)}\right]\right] = \frac{k\frac{dx}{dt}}{(k-x(t))x(t)}$

$$\begin{aligned} C &= \frac{\rho}{A}\frac{d\ln\left[\frac{\rho}{\rho_i-\rho}\right]}{dt} \\ &= \frac{\rho}{A}\frac{\rho_i}{\rho(\rho_i-\rho)}\frac{d\rho}{dt} \\ &= \frac{1}{A}\frac{\rho_i}{\rho_i-\rho}\frac{d\rho}{dt} \end{aligned}$$

leading to

$$\frac{d\rho}{dt} = \frac{CA}{\rho_i}(\rho_i - \rho) \tag{2.4a}$$

$$\frac{d\rho}{dt} = \frac{C'A}{\rho_i}(\rho_i - \rho) \tag{2.4b}$$

To continue from here two assumptions are made. The first is that the temperature and the accumulation rate dependencies may be separated, and that they thereby have no inter-correlation. The second is that the rate equations may be written as:

$$\frac{d\rho}{dt} = k_0 A^a(\rho_i - \rho), \rho < 0.55 \tag{2.5a}$$

$$\frac{d\rho}{dt} = k_1 A^b(\rho_i - \rho), 0.55 < \rho < 0.8 \tag{2.5b}$$

where k_0 and k_1 are Arrhenius type rate constants which are only temperature dependent, and a and b are constants determining the significance of the accumulation rate and are dependent on the densification mechanisms.
a and b may be determined by comparing slopes for densification at different sites of nearly equivalent conditions as:

$$a = \frac{\ln\left(\frac{C_1}{C_2}\right)}{\ln\left(\frac{A_1}{A_2}\right)} + 1 \tag{2.6}$$

and equivalently for b, with C_1' and C_2'.
k_0 and k_1 can be estimated by observing values of k at different temperatures and plotting $\ln(k)$ versus temperature - a so-called Arrhenius plot(REFERENCES) - to find A and E_a in equations:

$$k = Ae^{-\frac{E_a}{k_B T}} = Ae^{-\frac{E_a}{RT}} \tag{2.7}$$

$$\ln(k) = \ln(A) - \frac{E_a}{R}\frac{1}{T}$$

leading to values of k_0 and k_1 of:

$$k_0 = 11e^{-\frac{10160}{RT}} \tag{2.8a}$$

$$k_1 = 575e^{-\frac{21400}{RT}} \tag{2.8b}$$

Depth-density and depth-age calculations
Assuming that temperature, annual accumulation rate and initial snow density are known, the following calculations can be made:

- Density at depth h, $\rho(h)$
- Depth at pore close-off, $\rho = 0.55$

- Depth-age relationship from surface to pore close-off (stage 1 and 2).

1. stage of densification: Depth-density profile:

$$\rho(h) = \frac{\rho_i Z_0}{1 + Z_0} \tag{2.9}$$

where $Z_0 = e^{\rho_i k_0 h + \ln\left[\frac{\rho_0}{\rho_i - \rho_0}\right]}$. In this segment, the depth-density is independent of accumulation rate. The critical density depth can be calculated as:

$$h_{0.55} = \frac{1}{\rho_i k_0}\left[\ln\left[\frac{0.55}{\rho_i - 0.55}\right] - \ln\left[\frac{\rho_0}{\rho_i - \rho_0}\right]\right] \tag{2.10}$$

and the age at close-off depth as:

$$t_{0.55} = \frac{1}{k_0 A}\ln\left[\frac{\rho_i - \rho_0}{\rho_i - 0.55}\right] \tag{2.11}$$

WHERE DOES THIS COME FROM? **2. stage of densificaion:** The depth-density profile

$$\rho(h) = \frac{\rho_i Z_1}{1 + Z_1} \tag{2.12}$$

where $Z_1 = e^{\rho_i k_1 (h - h_{0.55})\frac{1}{A^{0.5}} + \ln\left[\frac{0.55}{\rho_i - 0.55}\right]}$. The age of firn at a given density ρ:

$$t_\rho = \frac{1}{k_1 A^{0.5}}\ln\left[\frac{\rho_1 - 0.55}{\rho_1 - \rho}\right] \tag{2.13}$$

An estimate of the mean annual accumulation rate can be made from the slope C' and the mean annual temperature:

$$A = \left(\frac{\rho_i k_1}{C'}\right)^2 \tag{2.14}$$

2.2.2 Diffusion

In Firn

Diffusion describes the attenuation of a given signal, e.g. a water isotopic signal, due to vapor phase diffusion in the porous firn column. To develop accurate knowledge of paleo climate and temperatures it is of great importance to understand this process, as a reconstruction of the part of the signal lost will reveal finer details in the signal and thus a more detailed knowledge of

past times. Diffusion can be described through Fick's 2nd law, which describes the change in concentration of a substance with time, due to diffusion:

$$\frac{\partial \phi}{\partial t} = D(t)\frac{\partial^2 \phi}{\partial z^2} - \dot{\epsilon}_z(t) z \frac{\partial \phi}{\partial z} \tag{2.15}$$

If we say the diffusion is focused on water isotopes, then we can approximate the water isotopic signal with the concentration, $\phi \approx \delta$, so:

$$\frac{\partial \delta}{\partial t} = D(t)\frac{\partial^2 \delta}{\partial z^2} - \dot{\epsilon}_z(t) z \frac{\partial \delta}{\partial z} \tag{2.16}$$

Through attanuation with depth and time due to diffusion there is a loss of information. But the diffusion constant and the vertical strain rate $\dot{\epsilon}_z(t)$ in Fick's 2nd law are dependent on temperature and accumulation on site, this information loss process can be used to infer temperature of firn and accumulation on site. The solution of Eq. 2.16 can be found by deconvolution. The attenuated, directly measured, isotopic signal, $\delta(z)$, can be described as the convolution between the initial isotopic signal, $\delta'(z)$, and a Gaussian filter, $\mathcal{G}(z)$, multiplied by the thinning function, $S(z)$, which describes the total thinning of a given layer at depth z due to the vertical strain from the above firn column.:

$$\delta(z) = S(z)[\delta'(z) * \mathcal{G}(z)] \tag{2.17}$$

where

$$S(z) = e^{\int_0^z \dot{\epsilon}_z(z')\, dz'} \tag{2.18}$$

and

$$\mathcal{G}(z) = \frac{1}{\sigma\sqrt{2\pi}} e^{-\frac{z^2}{2\sigma^2}} \tag{2.19}$$

In the gaussian filter, the variance σ^2 is referred to commonly as the diffusion length: the distance a water molecule is displaced along the z-axis. This quantity is directly related to both $D(t)$ and $\dot{\epsilon}_z(t)$(the strain rate being approximately proportional to the densification rate in the column). Thus an accurate estimate of the diffusion length is crucial for describing the diffusion process. The change of diffusion length over time is given as

$$\frac{d\sigma^2}{dt} - 2\dot{\epsilon}_z(t)\sigma^2 = 2D(t) \tag{2.20}$$

given by JOHNSEN1977, which also states that for the strain rate, the following approximation can be made:

$$\dot{\epsilon}_z(t) \approx -\frac{d\rho}{dt}\frac{1}{\rho} \tag{2.21}$$

where ρ is the density and $\frac{d\rho}{dt}$ is the densification rate. With this approximation, the solution to the equation for evolution of the diffusion length in the firn column can be found, defined only through density and densification rate, as(DESCRIBE HOW TO SOLVE FOR SIGMA):

$$\sigma^2(\rho) = \frac{1}{\rho^2} \int_{\rho_0}^{\rho} 2\rho'^2 \left(\frac{d\rho'}{dt}\right)^{-1} D(\rho')\, d\rho' \tag{2.22}$$

Certain densities and corresponding depths are of special interest as they indicate a specific stage of the firn and ice column. At top and bottom, we find the two extremum densities of settled snow, $\rho_{\text{snow}} = 330\frac{\text{kg}}{\text{m}^3}$, and ice, $\rho_{\text{ice}} = 917\frac{\text{kg}}{\text{m}^3}$. In between these two there are two more densities of importance: the critical density, $\rho_{\text{Cr}} = 550\frac{\text{kg}}{\text{m}^3}$, describing the transition between the two firn stages (see Section 2.2.1), and the pore close off density, $\rho_{\text{CO}} = 330\frac{\text{kg}}{\text{m}^3}$, describing the density at which air pockets in firn will seal of from each other to form single bubbles. From the close off density, further densification will be due to compression of these closed off air bubbles until the density reaches ρ_{ice}. If we assume that the diffusion constant, $D(\rho)$, and the densification rate, $\frac{d\rho}{dt}$ are known, then it is possible to give an estimate of the diffusion length profile by integrating from top, at density ρ_0, to pore close-off depth, ρ_{co}.

In Solid Phase

When firn reaches solid state, below close-off depth, the isotope diffusion is driven not as much by densification any more, but by isotopic gradients within the ice crystal lattice structure. This diffusion process is much slower than the diffusion in vapor phase taking place in firn, and thus does not contribute as much to the information loss and attenuation of the signal. For solid ice, at $\rho \leq \rho_{\text{ice}}$, the diffusion constant is only dependent on temperature, and can be described through an Arrhenius type equation as(ref: RAMSEIER1967, JOHNSENetal2000):

$$D_{ice} = 9.2 \cdot 10^{-4} e^{-\frac{7186}{T}} \left[\frac{\text{m}^2}{\text{s}}\right] \tag{2.23}$$

The diffusion length in ice ice given from the diffusion constant in ice and the thinning function as:

$$\sigma^2_{\text{ice}}(t) = S(t)^2 \int_0^t 2D_{\text{ice}}(t')S(t')^{-2}\, dt' \tag{2.24}$$

(DESCRIBE HOW TO SOLVE FOR SIGMA and a discussion of the ice diffusion constant.)

Reconstruction of temperatures

Reconstruction of paleotemperatures can be attempted through a number of various techniques (REFERENCES). For precise and accurate results, the single isotopelogue diffusion methods have proven useful(REFERENCES).
As is known, convolution in time domain is equal to multiplication in the frequency domain. According to equation (2.17), the transfer function to the frequency domain, will be the Fourier transform of the Gaussian filter:

$$\mathcal{F}[\mathcal{G}(z)] = \hat{\mathcal{G}} = e^{-\frac{k^2\sigma^2}{2}}, \qquad k = 2\pi f = \frac{2\pi}{\Delta} \tag{2.25}$$

where Δ is the discrete sampling size. This filter keeps larger wavelength frequencies (¿ 50 cm) unaltered but attenuates short wavelengths (¡ 20 cm) heavily, which is exactly the effect of diffusion on the isotopic signal. An estimate of the diffusion length σ^2 can be made from the power spectral density(PSD) of an isotopic time series. In the frequency domain a PSD composed of an initial signal, a filter function and a noise term is given by:

$$P_s = P_0(k)e^{-k^2\sigma^2} + |\hat{\eta}(k)|^2, \qquad f \in [0, f_{Nq}] \tag{2.26}$$

where the diffused and noise-affected signal, P_s, is equal to the original signal, $P_0(k)$, times a filter, $e^{-k^2\sigma^2}$ (our previously inspected Gaussian filter), plus a noise term, $|\hat{\eta}(k)|^2$, over a frequency space ranging from zero to the Nyquist frequency, f_{Nq}. The Nyquist frequency is dependent on the sampling resolution by $f_{Nq} = \frac{1}{2\Delta}$. The noise term, often categorized as white noise, but red noise is also seen in isotopic signals(REFERENCES), is given as

$$|\hat{\eta}(k)|^2 = \frac{\sigma_n^2\Delta}{|1 - a_1\, e^{ik\Delta}|^2} \tag{2.27}$$

Equation 2.27 describes an autoregressive process of the first order, with a_1 being an AR-1 coefficient. WHAT IS THIS? DESCRIBE..
The spectral estimate of the time series, $\mathbb{P}_s$, can be computed via a number of different numerical schemes, here Burg's method will be used, REFERENCES.
To determine the diffusion length a fit to these estimated spectral data, P_s, is found through for example a least square optimization, from which the parameters P_0, σ, a_1, σ_η^2 can be estimated.
The diffusion length σ^2 can be calculated by least-square minimization of the misfit between $\mathbb{P}_s$ and P_s.
This estimated diffusion length needs to be corrected: the obtained $\hat{\sigma}^2$ is affected by two further diffusion processes, taking place respectively in the ice and in the experimental sampling:

- **Sampling diffusion**: This diffusion is due to the sampling method. Sampling at a certain discrete resolution - be it discrete sections or resolution in CFA system due to step or impulse response - gives an additional diffusion length of

$$\sigma_{dis} = \frac{2\Delta^2}{\pi^2} \ln\left(\frac{\pi}{2}\right) \tag{2.28}$$

- **Ice diffusion** When below the close-off depth, a correction for the ice diffusion must also be made.

So to obtain the actual diffusion length from the raw data, both the sampling and the ice diffusion need to be subtracted from σ^2, and a scaling factor due to thinning from the strain must be introduced:

$$\sigma^2_{\text{firn}} = \frac{1}{S(z)^2}\hat{\sigma}^2_{\text{firn}} = \frac{\hat{\sigma}^2 - \sigma^2_{\text{dis}} - \sigma^2_{\text{ice}}}{S(z)^2} \tag{2.29}$$

Now, from the obtained estimate of the firn diffusion length, a temperature estimate can be made by numerically finding the root of:

$$\left(\frac{\rho_{co}}{\rho_i}\right)^2 \sigma^2(\rho = \rho_{co}, T(z), A(z)) - \sigma^2_{\text{firn}} = 0 \tag{2.30}$$

NOTE: Annual spectral signals appearing as peaks in the PSD, can influence the estimate of diffusion lengths. This can be taken into account by introducing a weight function omitting the annual signal from the PSD:

$$w(f) = \begin{cases} 0, & f_\lambda - df_\lambda \leq f \leq f_\lambda + df_\lambda \\ 1, & f < f_\lambda - df_\lambda, f > f_\lambda + df_\lambda \end{cases} \tag{2.31}$$

2.3 ECM and DEP

Electrical conductivity measurements(ECM), dielectric profiling(DEP) and isotopic composition analysis are three distinct ways of analyzing an ice core to examine past temperatures, climate and atmospheric composition. Some of these methods are sensitive to violent volcanic eruptions, which makes it possible to use known eruptions visible in the ice cores as volcanic horizons, and thus making dating of the ice core more precise and absolute.

2.3.1 Electrical Conductivity Measurements

The conductivity of ice arises from the current emerging due to the build-up of space charges in the ice structure. This conductivity can be analyzed by measuring the electrical current(DC) - induced by the electric potential and the acid balance - between two electrodes which are moved along the ice cores length. This current will be connected to the acid impurity concentration (pH), in the form of H_3O^+ concentration, of the ice core. Higher levels of acid impurity concentration are due to volcanic eruptions. Large amounts of volcanic gases, i.e. SO_2, in the atmosphere oxidizes and combines with water to form acid, i.e. sulphuric acid, which is the washed out of the air due to precipitation. Thus it is made possible to recognize volcanic horizons in ice cores, and - if the location of the eruption is known - from the amount of acid, the magnitude of the eruption can also be estimated.
High acidity of layers containing volcanic fall-out influence the dielectric constant of ice, so that these layers may be a possible explanation to the internal reflection horizons found in radio-echo sounding.
The measured current can then be transformed into acidity by a calibration curve relating the current, in μA, to the acidity, in μequivalents H_3O^+ per kilogram. To find the calibration parameters, the current and the acidity must be measured - the current through the above mentioned method, and the acidity through pH measurements of melted ice core samples. The pH measurements must further be corrected for any CO_2 induced H^+ ions (REFERENCES).The relation between acidity $[H^+]$ (corrected for CO_2 induced H^+) and current I can be expressed in two ways:

- $[H^+] = (0.017\, I^2 + 1.2)\mu$equiv. H^+/kg
  without a 50% correction for CO_2 surplus.

- $[H^+] = (0.045\, I^{1.73})\mu$equiv. H^+/kg
  with a 50% correction for CO_2 surplus.

The salt concentration in the ice can be estimated from measurements of the specific conductivity σ of the melted samples. The salt contribution hereto can be expressed as:

$$\sigma_s = \sigma - \sigma(H^+) - \sigma(X^-) - \sigma(HCO_3^-) \tag{2.32}$$

where the three later terms correspond to the contributions from H^+(through pH measurements) and its anions[1], HCO_3^- and any other anions X^-. The anion concentration will be equal to the cation concentration, which in this case

is only H^+ concentration. Disregarding low acidity samples, the concentration of HCO_3^- is negligible and thus concentration(X^-) $\approx$ concentration(H^+). The current is thus heavily influenced on/determined by the H^+ concentration, and thus it is approximated that the salt concentration has no influence on the current readings, which is fortunate, since the ECM method only responds to acidity, and not to salt and ammonia concentrations. This is one of the methods limitations, which the later dielectric profiling method took into account.

2.3.2 Dielectric Profiling

A method was later developed to demonstrate how both acids and salts play a decisive role in the determination of the electrical behavior of ice. The dielectric response of an ice core can be used to determine the total ionic concentration of the core. For ECM the measurements are sensitive to the fluctuating distance between ice core and electrodes, and after each measurement a fresh piece of ice needs to be prepared to repeat a measurement.
A new dielectric profiling technique (DEP) was developed (REFERENCES) with the advantages over the ECM that no direct contact is needed between the electrodes and the ice, so that the ice can stay in a protective polythene sleeve and the experiment easily can be repeated on the same piece of ice. Together the ice core and the polythene sleeve creates a complete system, where the plastic acts as an electrical blocking layer.
The dielectric response is measured by a sweeping of the AF-LF frequency range for the entire ice-polythene system. At LF the conductivity of the composite system is within a few percentages of the intrinsic behavior of the ice itself. At HF-VHF frequencies it also approximates well enough (REFERENCES).
The measured dielectric parameters are the conductivity of ice at HF-VHF range, denoted σ_∞ where ∞ signifies a frequency much higher than the relaxation frequency, f_r, of the dominant dispersion in the system. Both of these parameters display clear chemical response signals which can be used either alone or in combination with other ice core analysis measurements like ECM and isotope analysis.
If the core under analysis is chemically analyzed for Na^+, Mg^{2+}, Cl^-, SO_4^{2-} and NO_3^-, a number of important parameters, which can be used to evaluate the response of the dielectric parameters, can be calculated(REFERENCES):

[2]Anions are molecules losing a number of electrons to become negatively charged. Cations are molecules that gain a number of electrons to become positively charged.

- The salt parameter, which represents the total marine cation concentration calculated with the assumed marine ratios as:

$$[\text{salt}] = 1.05([\text{Na}^+] + [\text{Mg}^{2+}]) \tag{2.33}$$

- XSO_4, the excess sulphate, which represents the amount the sulphate concentration is above the expected if the salt and sulphate ions were in normal sea salt ratios. Excess sulphate is essentially sulphuric acid, which is the main acidic component of the ice.

- The strong acid content of the ice has been calculated as(assuming no other ions present in significant quantities):

$$[\text{acid}] = [\text{Cl}^-] + [\text{SO}_4^{2-}] + [\text{NO}_3^-] - 1.05([\text{Na}^+] + [\text{Mg}^{2+}]) \tag{2.34}$$

From data, it can be seen that acid and salt concentration peaks clearly affect σ_∞ and f_r(EXAMPLES, REFERENCES). The relationship between salt and acid, and the two dielectric parameters have been derived through non-linear regression analysis. In PAPER(REFERENCES) the linear responses for the DEP at -22°C were:

$$\sigma_\infty = (0.39 \pm 0.01)[\text{salt}] + (1.43 \pm 0.05)[\text{acid}] + (12.7 \pm 0.3) \tag{2.35}$$

with 76.6 % variance

$$f_r = (440 \pm 11)[\text{salt}] + (612 \pm 65)[\text{acid}] + (8200 \pm 400) \tag{2.36}$$

with 68.4 % variance. σ_∞ is measured in μS/m, f_r in Hz and [acid] and [salt] in μEq/l. The total ionic concentration of the ice core is strongly linked to the dielectric parameters, and a regression between the total anion concentration and the dielectric parameters gives:

$$[\text{anions}] = [\text{salt}] + [\text{acid}] = 0.022\sigma_\infty^{1.89} + 10^{-6} f_r^{1.61} - 0.2 \tag{2.37}$$

with 86.7 % variance.

The DEP complements the ECM technique by not only reacting to acids alone, as ECM does, but responds to both neutral salts and acids. The acid term is here associated with the DC conductivity, the same way it is also detected by ECM. The dielectric dependence on salts is consistent with the Bjerrum L defect[2]affecting every one or two salt ions in the ice, indicating

that a large fraction of the neutral salt is incorporated into the ice lattice. [3] The sensitivity to salt concentrations allows for identifications of periods with major storms and open seas which are also important identifiers for paleo climate research, along with the volcanic eruption detection made possible through the ECM.

2.4 Dating of Ice Cores Through Volcanic Horizons

Throughout the history of the earth a number of different geophysicals events have left their mark on the geological and glaciological records we use to steal a glance into the past. When considering ice core records, there are few as visible - both to the eye and in measured data - than volcanic eruptions. It is widely known [REFERENCE] that eruptions above a certain scale have the possibility to change not only the atmospheric composition, due to the heavy amount of volcanic material slung into the air, but also the ability to impact the climate in the years following an enormous eruption. Through electrical conductivity measurements it is possible to observe the very clear effects of some volcanic events in ice cores. Particles from the eruption are quickly transported from the source, since the atmospheric airflow will scatter the particles all over the atmosphere at a relatively high speed. Thus the dust(particle) and ECM signals pick up the volcanic signal faster than for example the isotopic signals. The isotopic signal reacts much slower, as it must be subjected to a change in global - and then following local - temperature, which might first show after a number of years. Thus ECM, DEP and dust measurements are good records to use for dating ice cores. Some eruptions are only great enough to show in ice cores located close to the volcanic source [REFERENCE], while others are of a magnitude impacting the entire globe, thus showing in almost all ice core records. These volcanic horizons are specifically good for synchronizing records, which is essential for developing knowledge about the geographically varying climate, temperatures and hemispherical dependency of the past. For this thesis the volcanic horizons are especially important for developing

[3] A Bjerrum defect is a crystallographic defect specific to ice, partly responsible for the electrical properties of ice. Usually a hydrogen bond will normally have one proton, but with a Bjerrum defect it will have either two protons (D defect) or no proton (L defect).(REFERENCES)

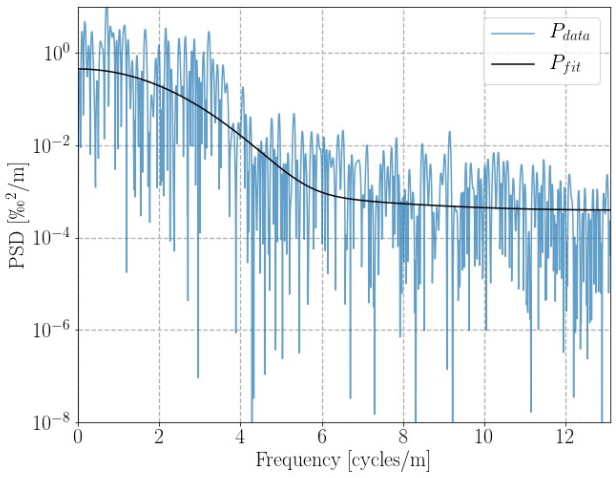

Figure 2.1: This is a great figure.

2.4.1 Laki and Tambora in Data and History

In the not-so-distant past two volcanic horizons have been of great importance for this thesis, namely the Laki eruption in 1783 and the Tambora eruption of 1815. Interestingly, these eruptions have not only impacted the geophysical world, but has left their footprints on the history of Man in politics[REFERENCE], sociology[REFERENCE], arts[REFERENCE] and philosophy[REFERENCE]. On the eighth day of June in 1783 a volcanic fissure located in the southern part of Iceland was central for a global climatic change. The fissure Lakagígar or more commonly known as Laki refering to the central mountain, erupted with violent phreagomagmatic explosions due to the basalt magma being exposed to ground water. The eruption was given a Volcanic Explosivity Index(VEI) of 4, corresponding to the magnitude of the much later 2010 Eyjafjallajökull Icelandic eruption. For the next eight months the fissure continued to emit great amounts of sulfuric aerosols into the atmosphere, resulting locally in Iceland in catastrophic mass famine, due to loss of livestock to poisoning, with up to 25 % of the population dying from starvation and poisoning from the volcanic gasses. Globally, the eruption caused a huge amount of sulfur dioxide to be spewed into the northern hemisphere which led to a global drop in temperatures and a generally more extreme climate. In the European regions the following summer was much warmer than usual with many thunderstorms to follow. The winter of 1783-84 was subsequently

extreme, with long periods of continuous frost. In France the late 1780's were marked by several years with droughts in the summer and frost in the winter, which contributed greatly to a rise in poverty and famine, and creating a greater division between the people and the rulers. Along with a growing dismay and distrust in the ruling forces the climatic changes due to Laki and a number of other climatic disruptions the French political situation finally climaxed in the French revolution of 1789. [REFERENCES!!!!]
32 years later on April 5 in 1815 an even more powerful eruption ensued: the eruption of Mount Tambora on the, now, Indonesian island Sumbawa. This eruption had a Volcanic Explosivity Index of 7, which makes it the most powerful in the recorded history of humankind. Considering that the VEI is defined as a logarithmic scale - at least for indices larger than VEI-3 - the Tambora eruption, though located just south of the Equator, impacted the entire globe as well as the European continent in at least the same magnitude as the 32 years prior Laki eruption. Locally, it was estimated to cause at least 10,000 direct deaths and many tens of thousands more due to sulfur dioxid poisoning, famine and disease. In many contexts the year of 1816 following the event became known as "*The Year Without a Summer*", as the ashes from the eruption column dispersed across the world and lowered global temperatures. This significant climate change though was not just a consequence of the Tambora eruption, but was pushed by a number of climatic forcings, some due to several previous volcanic activities around the globe. Combined, these effects coincided in a drop in global temperature by about 0.4 to 0.7 °C. This climatic change affected the entire globe by disrupting the Indian monsoons, causing a number of failed harvests, laying ground to severe typhus epidemics in southeast Europe and destroying crops and causing potato, oat and what harvest failure, especially in Ireland. Since the eruption had so severe consequences for the day to day lives of many people, the aftermath all around the world has been one of the greatest documented in recorded time, with a clear impact on the works of many artists, among them Lord Byron and J. M. W Turner[REFERENCES!!!!]. Although both eruptions caused many a tragedy, there is beauty in using these events as volcanic horizons in ice core records. Given the severity of both eruptions, they have been so well documented in historical records that they make up solid and certain pillars in developing a temporal map of the past life of our ever so active earth. For that and for their brutal beauty they will remain in human history for a great while to come.

Chapter 3

Isotopic Data: Laki to Tambora as seen in N Ice Cores.

3.1 Selection of Data

3.1.1 AWI B-cores

3.1.2 Crete and Surrounding Alphabet Cores

3.2 Interpolation

3.3 Data Specifications

Chapter 4

Signal Restoration and Peak Detection

The data obtained through various experimental measurements are easily compared with a time series, as they typically show some quantity measured all along the depth of an ice core. This depth is often, at short intervals, treated as a regular linear time series thus making it possible to use some of the known signal analysis methods. Of course, when considering the entirety of an ice core, the linearity disappears as thinning and compression makes the depth series non linear. But when considering short lengths of core it is possible to estimate a linearity, assuming conformity in this specific layer.

4.1 Back Diffusion

Due to diffusion in firn and ice, some of the water isotopic signal is lost. Some of this signal can be restored by investigating the diffusion process, and through filtering and deconvolution techniques(REFERENCES). For the data of this thesis two different restoration techniques are presented: a spectral method, determining the effect of mixing and diffusion as a spectral filter(REFERENCES), and a kernel restoration method much like the ones used to restore pixel resolution in images (REFERENCES).

4.1.1 Spectral Analysis

Power Spectral Densities

A very useful tool for analyzing signals exhibiting oscillatory effects is analysis of the signals power spectrum. Instead of considering the signal in time, it is

transformed to the spectral domain, where it is possible to obtain an estimate of both the signal and the underlying noise. This is crucial for enhancing the signal and filtering away noise. But to be able to examine these effects, first the data must be transformed. A range of different methods may be used to compute the frequency transform of the depth series, here I present the three I have been working with. Since the data are discrete and experimental, I will be presenting the discrete and applicable mathematical models.
When considering a signal, it may be of interest to investigate how the energy of said signal is distributed with frequency. The total power is defined as:

$$\text{Total Power} = \int_{-\infty}^{\infty} |X(\tau)|^2 \, d\tau. \tag{4.1}$$

Using Parseval's theorem (REFERENCE) (assuming that the signal has a finite total energy), the power of the signal can alternatively be written as

$$\int_{-\infty}^{\infty} |X(\tau)|^2 \, d\tau = \int_{-\infty}^{\infty} |\tilde{X}(\tau)|^2 \, df \tag{4.2}$$

where $\tilde{X}(f)$ is the spectral (Fourier) transform of the signal, from time to frequency domain, defined as:

$$\tilde{X}(f) = \int_{-\infty}^{\infty} X(\tau) e^{2\pi i f \tau} \, d\tau \tag{4.3}$$

and the inverse spectral (Fourier) transform, from frequency to time domain, defined as:

$$X(t) = \int_{-\infty}^{\infty} \tilde{X}(f) e^{-2\pi i f \tau} \, df. \tag{4.4}$$

Both $X(t)$ and $\tilde{X}(f)$ represent the same function, just in different variable domains. Often, the angular frequency ω is used instead, with the relation between ω and f being $\omega \equiv 2\pi f$, giving the Fourier and inverse Fourier transforms as:

$$\begin{aligned} \tilde{X}(\omega) &= \int_{-\infty}^{\infty} X(t) e^{i\omega\tau} \, d\tau \\ X(\tau) &= \int_{-\infty}^{\infty} \tilde{X}(\omega) e^{-i\omega\tau} \, d\omega \end{aligned} \tag{4.5}$$

From Equation 4.2 we can interpret the integrand on the right hand side $|\tilde{X}(f)|^2$ as a density function, describing the energy per unit frequency. This

is a property which is able to reveal much information about the considered signal, and it is useful to define this as the (one-sided) Power Spectral Density:

$$P_X(f) \equiv |\tilde{X}(f)|^2 + |\tilde{X}(-f)|^2 \qquad 0 \leq f < \infty \tag{4.6}$$

This entity ensures that the total power is found just by integrating over $P_X(f)$ from 0 to ∞. When the function is purely real, the PSD reduces to $P_X(f) = 2|\tilde{X}(f)|^2$.
In the above the transform used to define the PSD was presented as the Fourier transform. When working with discrete data, as is very common when analyzing real world data, there are a number of different ways of estimating the PSD. In the following three different methods will be presented, all used in this thesis.

RETHINK THIS PART. DO NOT USE TIME ON ALL THE CALCULATIONS. WRITE THE GENERAL IDEAS OF THE METHODS AND STATE HOW TO CALCULATE/COMPUTE. SMALL CODE SNIP TO GIVE GENERAL IDEA.

Discrete and Fast Fourier Transform

The definition of the continuous Fourier transform and its inverse was presented in the above. The Fourier transform is as seen a way of representing the function under consideration as an infinite sum of periodic components. When the function is discrete, so will the Fourier transform be, and the integral is replaced with a sum. This gives us the Discrete Fourier Transform (DFT) which transforms the signal into a sum of separate components contributing at different frequencies. The DFT is dependent on the sampling interval, Δ, and we can describe our discrete signal X as a function of N discrete time steps $t_k = k \cdot \Delta$, where $k = 0, 1, ..., N - 1$:

$$X_k \equiv X(t_k) \tag{4.7}$$

This sample size is supposed to be representative for the entire discrete function, if the function continues beyond the N sampled points. When sampling discretely at interval Δ, there will be a special frequency, the Nyquist critical frequency, defined through the sampling size as:

$$f_{NQ} \equiv \frac{1}{2\Delta}. \tag{4.8}$$

This frequency is of great importance in transformation of discrete signals. If the continuous signal is sampled at an interval Δ is bandwidth limited to frequencies smaller in magnitude than f_{NQ}, $\tilde{X}(f) = 0$ for $|f| \geq f_{NQ}$ - i.e. the transformed function has only non-zero values inside the Nyquist interval, $\tilde{X}(-f_{NQ}), ..., \tilde{X}(f), ..., \tilde{X}(f_{NQ})$. This means that the function is completely determined since we have all information about the signal contained in our available frequency space.
On the other hand, which is much more likely, if the continuous signal consists of frequencies both inside and outside the Nyquist interval, then all spectral information outside of this range will be falsely interpreted as being inside this range. Thus a wave inside the interval with a frequency of f_n will have a number of wave siblings outside of the interval, with frequencies of $k \cdot \frac{1}{\Delta} f_n$, k being integers, which will be aliased into the Nyquist interval and give rise to an increased power at the frequency f_n.
When analyzing an already measured discrete signal, this might give rise to some headache. What can be done is to assume that the signal has been sampled competently and then assume that the Fourier transform is zero outside of the Nyquist interval. After the analysis it will then be possible to determine if the signal was indeed competently sampled, as the Fourier series will go to zero at f_{NQ} given a correct assumption, and go to a fixed value, if the sampling was not done competently.
Now with the basics of understanding the limits of frequency transform of a discretely sampled signal, it is possible to estimate the DFT of the signal $X_k \equiv X(t_k)$. Since the Fourier transform is a symmetric transformation it is easiest to assume that N is even.

Since the input information is of size N we should expect only to sample the frequency transform $\tilde{X}(f)$ at only discrete values of f in the range between the upper and lower critical Nyquist frequencies, $-f_{NQ}$ to f_{NQ}:

$$f_n \equiv \frac{n}{N\Delta}, \qquad n = -\frac{N}{2}, ..., \frac{N}{2} \tag{4.9}$$

This will indeed actually give rise to $N + 1$ values, since 0 will be in the interval as well, but the limit frequencies are actually not independent, but all frequencies between are, which reduces it to N samples.
Now the integral from Equation 4.3 needs to be estimated as a sum:

$$\tilde{X}(f_n) = \int_{-\infty}^{\infty} X(\tau) e^{2\pi i f_n \tau} dt \approx \sum_{k=0}^{N-1} X_k e^{2\pi i f_n t_k} \Delta = \Delta \sum_{k=0}^{N-1} X_k e^{2\pi i k \frac{n}{N}} \tag{4.10}$$

The Discrete Fourier Transform is thsu defined as:

$$\tilde{X}_n \equiv \sum_{k=0}^{N-1} X_k e^{2\pi i k \frac{n}{N}} \tag{4.11}$$

This gives the approximate relation between the DFT estimate and the continuous Fourier transform $\tilde{X}(f)$ when sampling at size Δ as:

$$\tilde{X}(f_n) \approx \Delta \tilde{X}_n \tag{4.12}$$

The inverse DFT is given as:

$$X_n \equiv \frac{1}{N} \sum_{n=0}^{N-1} X \tilde{X}_n e^{-2\pi i k \frac{n}{N}} \tag{4.13}$$

Computation of the DFT can be very slow and tiresome, since it involves complex multiplication between a number of vectors and matrices. If we write Equation 4.11 as $\tilde{X}_n = \sum_{k=0} N - 1 W^{nk} X_k$, where W is a complex number $W \equiv e^{2\pi i/N}$. This shows that the vector X_k must be multiplied with a complex matrix which (n,k)th component consists of the constant W to the power of nk. This matrix multiplication evidently leads to a process of $O(N^2)$. Fortunately, a number of different algorithms(REFERENCES) have been developed for fast and efficient computation of the discrete Fourier transform. One of these is called the Fast Fourier Transform (FFT), which can reduce the computations to just $O(N \log_2 N)$! In this thesis the FFT used is the one implemented in the numpy.fft Python package(REFERENCES) which is based on the works of (REFERENCES). See said article for implementation details. One important thing about this specific algorithm is that for the algorithm to function most efficiently, the number of points computed in the frequency space must be of a power of 2, following the use of base $\log_2$

Discrete Cosine Transform

The DFT is generally defined for complex inputs and outputs, where the sine components of the transform describe the complex part and the cosine describes the real part.
Since the data analyzed in this thesis is purely real, it makes sense, for computational speed, to only work with the cosine parts of the transform. This leads to the Discrete Cosine Transform (DCT) which transforms real inputs to real outputs.

4.1.2 Spectral Filtering

Wiener Filtering

Through spectral analysis it is possible to treat the noise of the signal consistently. The goal is to create spectral filters which enhances the signal while minimizing the effect of the noise, thus increasing the signal-to-noise ratio (SNR).
Theoretically, without any diffusion, the change in isotopic concentration would be described through a step function, going from one constant concentration to another. This step function can be described by the Heaviside function:

$$D(t) = \begin{cases} 0, & t < 0 \\ 1, & t \geq \end{cases} \tag{4.14}$$

In reality, a number of different mixing processes change this step function, and the measured signal will be a smooth curve, $s(t)$, which corresponds to the convolution of $S(t)$ with the mixing response function $M(\tau)$

$$d(t) = \int_{-\infty}^{\infty} D(\tau) \cdot M(t - \tau) d\tau \tag{4.15}$$

4.1.3 Signal Restoration by Optimal Diffusion Length

Kernel Estimation

As is well known, in the spectral domain, convolution is multiplication and the mixing is described as the multiplication between the Fourier transform of S and M:

$$\tilde{d} = \tilde{D} \cdot \tilde{M} \tag{4.16}$$

By differentiation with respect to time, the mixing filter M is unaffected, and differentiation of the measured system response, the Heaviside function, S' is a delta function, which Fourier transformed is unity, leading to:

$$\tilde{d'} = \tilde{D'} \cdot \tilde{M} = \tilde{M} \tag{4.17}$$

The mixing filter can thus be determined by measuring the system response to a step function, differentiating performing Fourier transform of the result d'.

After determination of the mixing filter $\tilde{M}$, the unmixed signal D can be estimated in theory by inverse Fourier transform of

$$\tilde{D} = \tilde{d} \cdot \tilde{M}^{-1} \tag{4.18}$$

During the mixing, cycles with short wavelengths are heavily washed out, and through the restoration in Eq. 4.18, the amplitudes corresponding to these wavelengths are heavily amplified by the filter. This method though has a drawback, which is that when the measurements contain noise, the restored signal will be dominated by high-frequency noise, greatly amplified by the mixing filter. Thus it is a problem of retaining as much (short wavelength) signal as possible while simultaneously attempting to amplify the high-frequency noise as little as possible. This optimal trade-off can be found by creating an optimum filter for the considered measured isotopic signal:

$$\delta_M(z) = \delta_m(z) + \eta(z) \tag{4.19}$$

This optimal (Wiener) filter $\tilde{F}$, defined for each wave number $k = 2\pi\omega$, is presented as the ratio between pure signal and pure signal plus noise described in Power Spectral Densities as:

$$\tilde{F}(k) = \frac{|\tilde{\delta_m}(\omega)|^2}{|\tilde{\delta_m}(\omega)|^2 + |\tilde{\eta}(\omega)|^2} \tag{4.20}$$

In this work, the power spectral densities of the signal and the noise, respectively, are determined through analysis of the power spectral density of the combined signal/noise PSD.
The PSD of the noise free measured signal, $|\tilde{\delta_m}(\omega)|^2$, is assumed describe as

$$|\tilde{\delta}_m(\omega)|^2 = P_0 e^{-k^2\sigma_{\text{tot}}^2} \tag{4.21}$$

where σ_{tot}^2 describes the total estimated diffusion length of the mixing.
The noise is assumed to be red noise, described by an autoregressive process of first order, AR1:

$$|\tilde{\eta}(\omega)|^2 = \frac{\sigma_\eta^2 \Delta z}{|1 + a_1 \exp(-2\pi i \omega \Delta z)|^2} \tag{4.22}$$

where σ_η^2 is the variance of the red noise, a_1 is the AR1 coefficient and Δz is the resolution of the time/depth data. It is then possible to estimate the parameters P_0, σ_{tot}^2, σ_η^2 and a_1 by curve fitting, separately, the two expressions in Eq. 4.21 and 4.22 to the data. The estimated parameters are varied to find the optimal guess to use for the filter.

4.2 Enhanced Resolution and Peak Detection

4.2.1 B Spline Multipolynomial Interpolation

4.2.2 Detrending and Standardising

4.2.3 Cycle Length Estimation of Detrended Signal

Chapter 5

Community Firn Model and Temperature Reconstruction

Hello

Chapter 6

Layer Counting and Annual Layer Thickness Estimation

Clevercleverclever

Chapter 7

General Method and Algorithm Walk-Throughs

This section contains a walk through of the method to back diffuse a given ice core depth series to attempt to restore as much of the original signal as possible. For now, the method has been developed for sections that has been dated to be between the two volcanic eruptions Laki and Tambora, as these are very well dated, and thus it is possible to find the optimal diffusion length to back diffuse with as the actual number of annual layers is exactly known for this data series. The method is easily modified for any other dated depth series, as what is needed is just the number of annual layers in the given data series.
Figure 7.1 shows a flowchart of the method used to estimate the diffusion length of a depth series with a preliminary guess of number of annual layers. In the following sections each of the steps in the method will be discussed more thoroughly and examples will be given, all based on the Greenlandic ice core drilled at Site A near Crete(REFERENCES!!!). The method is built such that it takes two inputs - the isotopic depth series, and the specifications for the particular ice core - and uses these for the first preliminary computations needed to make a first, naïve guess of the diffusion length, σ_0. This diffusion length is then used to deconvolute the data and give a first estimate of the number of peaks in the data series. If this number is different from the already specified number of annual layers - in this case 32 - then the diffusion length will be updated accordingly: If the counted number is higher(lower) than the actual number, the diffusion length is adjusted downwards(upwards) with $\Delta\sigma_2$ and the deconvolution and peak counting is performed again. On the other hand, if the counted number is equal to the actual number, then the diffusion

length is optimized to find the largest diffusion length which still gives the actual number of counted peaks. When this σ_{final} is reached, the algorithm stops and returns the final diffusion length estimate along with the associated back diffused depth series.

7.0.1 Input

To compute the final diffusion length and depth series, two inputs are needed: the measured isotopic depth series and the specifications of the examined core. Through this section all examples have been carried out using the core Site A.

Core	Drilled	Core length	Geographic position		Elevation	Laki	Tambora	Mean accum. rate	Temp. at 10m	Temp at 20m
			Latitude	Longitude						
ID	[Yr]	[m]	[°N]	[°E]	[m a.s.l.]	[m]	[m]	[m ice/Yr]	[°C]	[°C]
Crete	1974	404.0	71.12	322.68	3172	74.75	64.70	0.280	-30.40	-30.16
Milcent	1973	398.0	70.30	315.00	2410			0.530	-22.30	-0.00
Camp C	1977	100.1	77.18	298.89	1880	91.50	78.50	0.380	-24.29	-24.35
SiteA	1985	128.6	70.63	324.18	3092	80.85	70.90	0.307	-29.41	-29.41
SiteB	1984	105.6	70.65	322.52	3138	83.70	73.00	0.327	-29.77	-29.48
SiteC	1984	24.9	70.68	321.21	3072			0.340	-29.10	-28.54
SiteD	1984	100.1	70.64	320.38	3018	93.80	81.50	0.365	-28.30	-27.89
SiteE	1985	77.8	71.76	324.15	3087	62.95	53.40	0.225	-30.37	-30.41
SiteF	1985	25.7	71.49	324.12	3092			0.237	-30.42	-30.36
SiteG	1985	70.8	71.15	324.16	3098	69.40	60.50	0.251	-30.10	-30.01
SiteH	1985	26.2	70.87	324.16	3102			0.277	-29.59	-29.53

Table 7.1: Overview of specifications of all examined Greenlandic ice cores.

In Figure 7.2 the depth series between the eruptions Laki and Tambora can be seen along with the entire ice core in the background. This is the diffused, measured raw data from Site A. Dating of the ice cores has been carried out by matching Electrical Conductivity Measurements (ECM, Section **??**) with water isotopic - in this case δ^{18}O - data measured at the same depths. By doing so it is possible to identify known volcanic horizons in the ECM data and thus getting a sharp marker of when the precipitation of that given depth fell. In Figure 7.3 the matched ECM and δ^{18}O profiles can be seen with Tambora marked at depth ____ and Laki at depth ____.

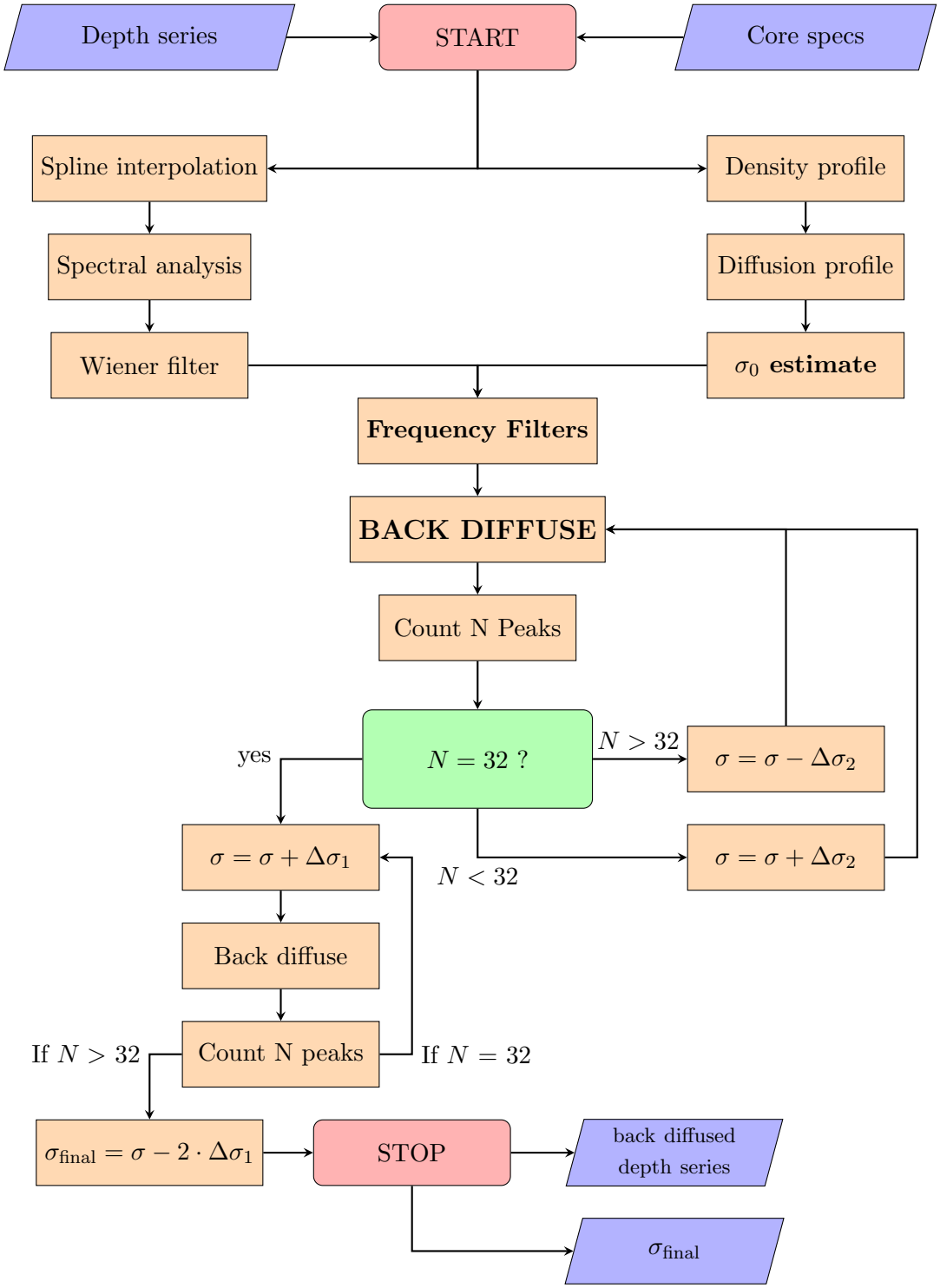

Figure 7.1: Flowchart of method for diffusion length computation.

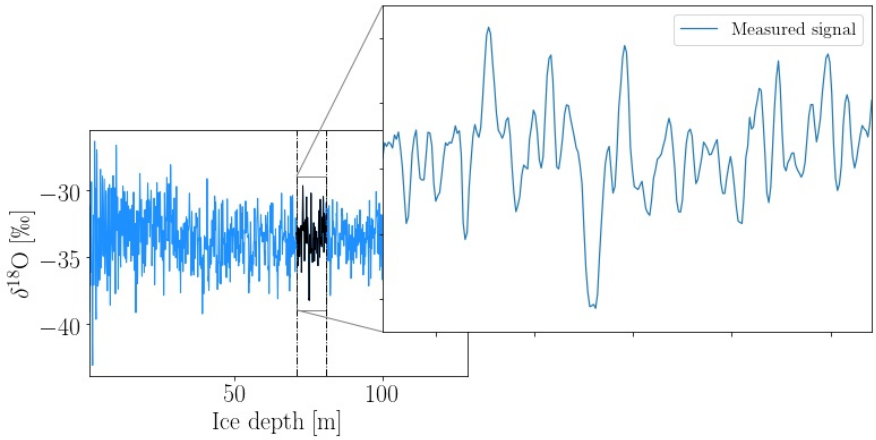

Figure 7.2: The entire ice core isotopic profile from Site A, with a zoom in on the estimated depth series spanning from Tambora to Laki.

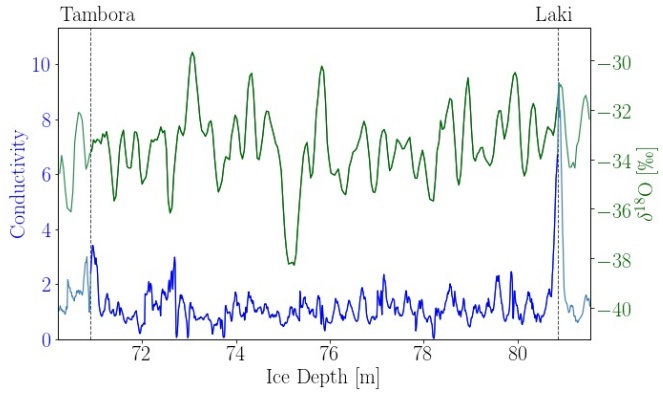

Figure 7.3: Two depth profiles from the core drilled at Site A showing accordingly the measured δ^{18}O isotopic values and the conductivity measurements in the depth ranging from the estimated Tambora eruption to the Laki eruption.

7.0.2 Preliminary Computations

From the inputs a number of preliminary computations need to be carried out before the optimization of the diffusion length can be performed. For the depth series this consists of first interolating the data to make sure that the depth series is evenly sampled, then an analysis of signal and noise in the frequency spectrum needs to be carried out, and from this spectral analysis

a Wiener filter can be constructed to find the optimal high frequency cut off, where as much noise as possible is filtered away while losing as little of the signal as possible. These computations are all based on the depth series data and use only signal analysis theory.
The input of core specifications on the other hand is used to give a more theoretical view of the situation. From these preliminary inputs, containing accumulation rate, borehole temperatures, altitudes and other conditions, it is possible to use ice core and ice flow theory to compute initial estimates of density and diffusion profiles at the given site. From these profiles along with the volcanic horizons indicating the series of interest, an initial estimate of the diffusion length at the depth of Laki to Tambora.
Firstly, the computations associated with inputted depth series are considered and later the ones associated with the core specifications are described.

Depth Series: Spline Interpolation

When working with ice core data, it is not always a certainty that the data you get from the field are as continuous or as evenly sampled as one could have hoped. A lot of factors are at play when drilling, transporting, dividing and cutting an ice core for laboratory studies. Some parts of an ice core contain brittle zones where the ice is likely to break, leaving a section almost impossible to analyze. When transporting the drilled ice cores they are susceptible to both melting and contamination and evaporation of the outermost ice layer of the core. And finally of course there is a number of uncertainties that occur when cutting an ice core into discrete bits to be measured. The quality of data varies rather greatly from site to site, from drill team to drill team and of course from laboratory to laboratory.

When looking at the depth series only it might not be an issue to have various spacing between the discrete measurements, but when it comes to spectral analysis, it is of necessity to obtain a depth series signal with an even distribution. To accommodate this need interpolation of the signal can be of use. In the case of the ice core drilled at Site A, it can be seen from Figure 7.4 that the raw measured signal has a minimum sampling size of $\Delta_{\min} = 0.038$ and a maximum sampling size of $\Delta_{\max} = 0.040$. To be able to analyze this signal in the spectral domain the signal can be numerically resampled with an even sampling rate. This is done by choosing the minimum sampling size available, $\Delta_{\min} = 0.038$, and redistributing the depth data points to be evenly spaced with this sampling size. The redistribution is carried out as follows.

Assuming the original depth array $\mathbf{d}$ is distributed as $d_{i-1} < d_i < d_{i+1}$ with $i = 0, ..., n-1$ has a minimum sampling distance as $\Delta_{\min}$ we define

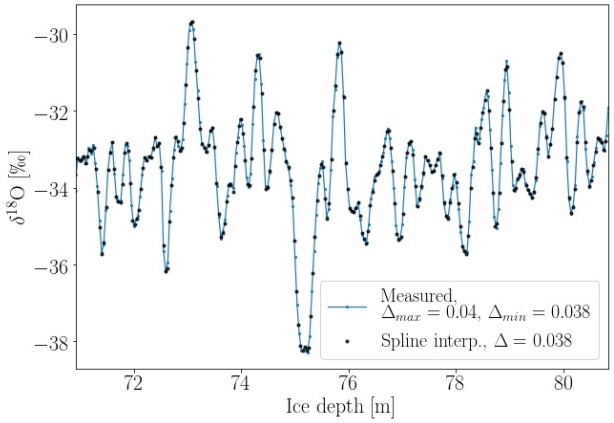

Figure 7.4: The unevenly measured data from Site A in the depth ranging from Tambora to Laki along with the now evenly sampled cubic spline interpolated data. Sampled with an interval of $\Delta = 0.038$.

the new sampling distance for the new depth array $\hat{\mathbf{d}}$ as $\Delta = \Delta_{\text{min}}$ - again assuming that $\hat{\mathbf{d}}_{j-1} < \hat{\mathbf{d}}_j < \hat{\mathbf{d}}_{j+1}$ with $j = 0, ..., \hat{n} - 1$. This makes it possible to define the first and last value of the new array as

$$\hat{\mathrm{d}}_0 = \Delta \lceil \frac{\mathrm{d}_0}{\Delta}, \rceil \tag{7.1}$$

$$\hat{\mathrm{d}}_{\hat{n}-1} = \Delta \lfloor \frac{\mathrm{d}_{n-1}}{\Delta} \rfloor. \tag{7.2}$$

From this the number of values in the new array, $\hat{n}$, can be determined as

$$\hat{n} = 1 + \frac{\hat{\mathrm{d}}_{\hat{n}-1} - \hat{\mathrm{d}}_0}{\Delta}, \qquad \hat{n} \in \mathbb{Z}. \tag{7.3}$$

Thus our new depth array will be given as

$$\hat{\mathbf{d}} = \hat{\mathrm{d}}_0 + j \cdot \Delta, \qquad j = 0, ..., \hat{n} - 1. \tag{7.4}$$

The original data are then used to define a cubic spline interpolation function to which the redistributed depth data points can be matched. For this part of the data analysis the `SciPy.interpolate` Python (REFERENCE) package with `SciPy.interpolate.CubicSpline` for the cubic spline interpolation. This gives a new distribution of data points as seen in Figure 7.4.

```
def interpCores(self, pad = 1):

    # Method in BackDiffuse class

    isoData = self.d18OData
    d_in = isoData['depth']
    x_in = isoData['d18O']


    if self.interpAll:
        valMin = d_in.min()
        valmax = d_in.max()
    else:
        valMin = self.depthMin - pad
        valMax = self.depthMax + pad


    d = d_in[(d_in >= valMin) & (d_in <= valMax)]
    x = x_in[(d_in >= valMin) & (d_in <= valMax)]

    diff = np.diff(d)
    Delta = round(min(diff), 3)

    d_min = Delta * np.ceil(d.values[0]/Delta)
    d_max = Delta * np.floor(d.values[-1]/Delta)

    n = int(1 + (d_max - d_min)/Delta)

    j_arr = np.linspace(0,n,n)
    dhat0 = d_min + (j_arr - 1)*Delta

    f = interpolate.CubicSpline(d,x)

    xhat0 = f(dhat0)

    dhat = dhat0[(dhat0 >= self.depthMin) & (dhat0 <= self.
    depthMax)]
    xhat = xhat0[(dhat0 >= self.depthMin) & (dhat0 <= self.
    depthMax)]

    return dhat, xhat, Delta
```

Listing 7.1: Spline interpolation of $\delta^{18}O$ data.

Depth Series: Spectral Analysis

Now with evenly spaced depth series data it is possible to transform the data to the frequency domain and perform spectral analysis on the signal. The

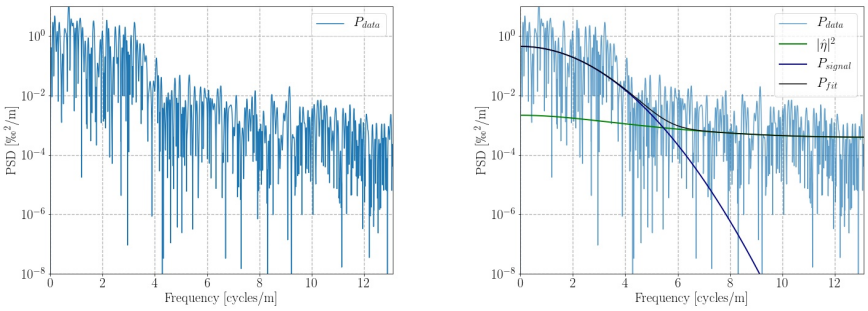

(a) **(b)**

Figure 7.5: Spectral Analysis. **(a)** The power spectral density(PSD) of the interpolated data from Site A shown in Figure 7.4. The PSD was computed through a Discrete Cosine Transform(DCT). **(b)** Spectral estimate of the depth series from Tambora to Laki along with fit to entire spectral data set and the separated estimates of the noise and signal functions, as described in section **??**

basic theory concerning Fast Fourier Transform(FFT), Discrete Cosine Transform(DCT) and Power Spectral Densities(PSD) is discussed in Section **??**. In this section the theory is merely put to use. Since the data under examination is completely real with no imaginary parts, pointing towards the sensibility of working only with cosines to enhance computational speed. Furthermore the DCT implies different boundary conditions than the FFT, meaning that some of the odd spectral behaviour, like aliasing can be avoided by using a different transform.

Make a comment on Nyquist frequncy.

For the depth series between Laki and Tambora at Site A, the PSD computed through the DCT as PSD = $|\text{DCT}|^2$ can be seen in Figure 7.5a. This spectrum shows a higher intensity in the low frequency area and a lower intensity at high frequencies indicating a low frequency signal and some high frequency noise.

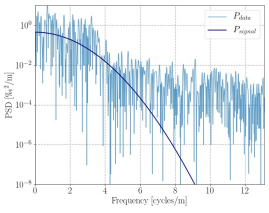

(a)

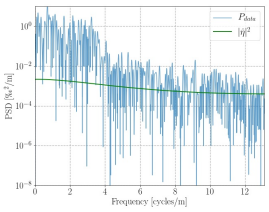

(b)

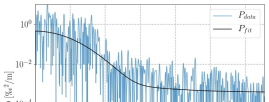

Since the signal is that of a real physical phenomena, and even one that we do have some acquaintance with, it is relevant to use some knowledge of the theory to describe the apparent spectrum, which has also been done in section **??**. Recalling the definitions of the noise and the signal as they are assumed to be based on the physical theory, it is possible to carry out a fitting routine to determine the parameters of the noise, signal and combined model function. This routine is performed in the following steps:

- Define the noise, signal and model functions to fit:

$$|\eta(\omega)|^2 = \frac{\sigma_\eta^2 \Delta z}{|1 + a_1 \exp(-2\pi i \omega \Delta z)|^2} \tag{7.5}$$

$$P_{\text{signal}}(k) = P_0 \cdot e^{-k^2 \sigma_{tot}^2} \tag{7.6}$$

$$P_{\text{model}} = |\eta(\omega)|^2 + P_{[}\text{signal}](\omega) \tag{7.7}$$

- Define two methods to calculate residuals between the measured data, $\boldsymbol{y}$, and the modelled estimate $\boldsymbol{m}$. The listings of these methods can be seen in Listings 7.2 and 7.3.

```
def calc_res(params, x, y, dt, weights):
    # Set parameters as input parameters
    P0, s_eta2, s_tot2, a1 = params

    # Define signal and noise function based on given params
    Noise = self.func_Noise(x, s_eta2, a1, dt)
    Signal = self.func_Signal(x, P0, s_tot2)

    # Define model as sum of noise and signal
    Pmod = Noise + Signal
    # Calculate (weighted) log residual
    res = weights*(np.log10(y) - np.log10(np.copy(Pmod)))

    return res
```

Listing 7.2: Residual calculations for spectral fit.

```
def sum2_res(params, x, y, dt, weights):

    # Calculate sum of the squared residuals.
    return np.sum(calc_res(params, x, y, dt, weights)**2)
```

Listing 7.3: Calculation of the sum of squared residuals.

- Define boundaries for the parameters examined: P_0, σ_η, σ_{tot}, a_1.
- Make initial parameter guess :
- Otimization routine to minimize residuals. This routine is carried out by using the Python package `sp.optimize.fmin_l_bfgs_b`, an optimization through the limited-memory BFGS bound constraint algorithm .

Write boundaries used - explain why.

Write initial guesses

REFERENCE!!! Maybe write more? No...

The signal, noise and combined fit can be seen separately in Figure 7.6a, 7.6b and 7.6c, respectively, and plotted together in Figure 7.5.

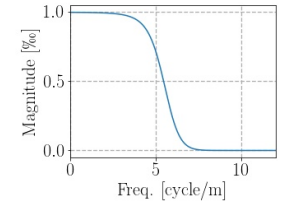

REFERENCE!!!

(a)

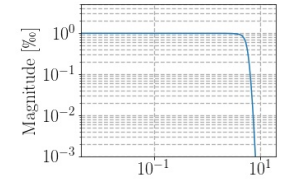

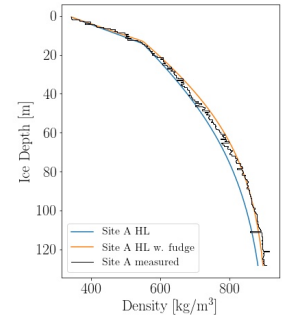

Figure 7.8: Depth density profile at Site A.

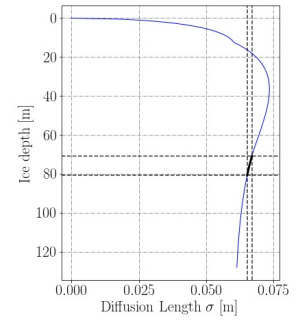

Figure 7.9: Estimated diffusion profile at Site A given a Herron Langway model.

Depth Series: Wiener Filter

When the optimal fit to the spectral data has been found, it is possible to construct an optimal filter to cut off as much high frequency noise as possible while still maintaining the most signal. This is commonly called a Wiener filter . Recalling from Section **??** this filter is described as the ratio between the signal alone and the signal plus noise model:

$$\tilde{F}(k) = \frac{P_{\text{signal}}(k)}{P_{\text{signal}}(k) + |\tilde{\eta}(k)|^2}. \tag{7.8}$$

This yields a filter that annihilates high frequencies above a certain cut but at the same time leaves room around this cut for both dampening low frequencies and not completely killing high frequencies in that area. This logistic curve can be seen plotted on a linear and a double logarithmic scale in Figures 7.7a and 7.7b respectively.

Core Specifications: Density Profile

Right here is something very imortant.

As well as here.

Core Specifications: Diffusion Profile

Core Specifications: σ_0 estimate

7.0.3 Back Diffusion/Deconvolution

7.0.4 Peak Counting

7.0.5 Decision Algorithm

7.0.6 Output

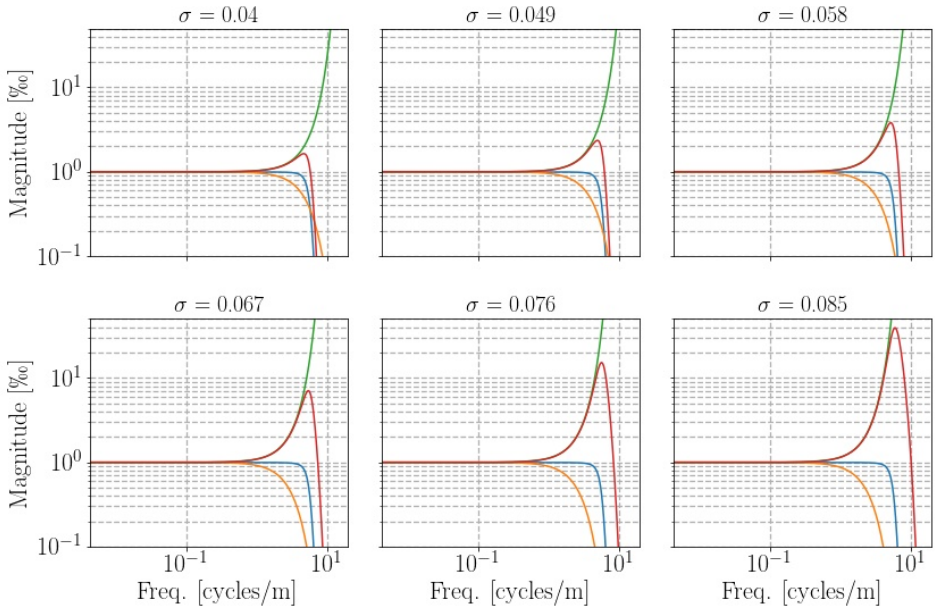

Figure 7.10: Frequency filter examples ranging from diffusion length 0.04 m to 0.085 m.

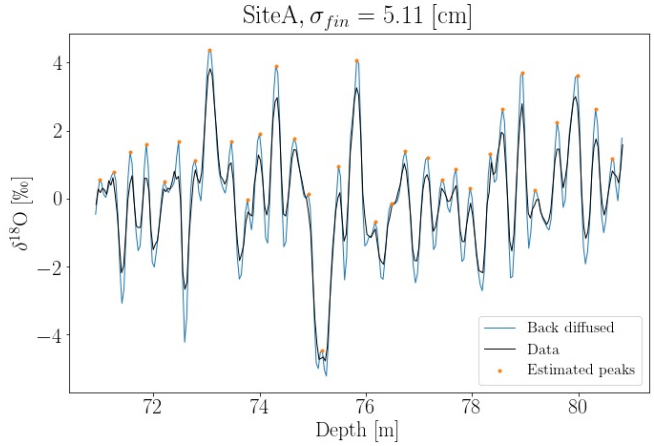

Figure 7.11: Best estimate of deconvoluted depth series given an annual count of 32 years - marked as orange dots. The best estimate is taken as the largest diffusion length that still yields 32 years in the depth span from Tambora to Laki.

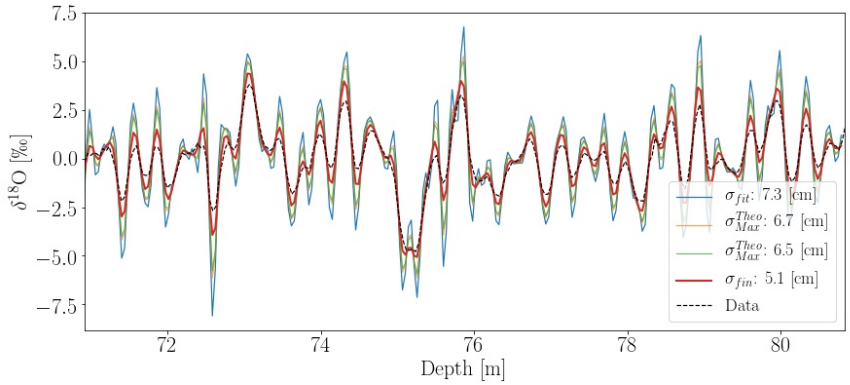

Figure 7.12: Estimated back diffused data series with different diffusion length estimates: diffusion length estimate from spectral fit (σ_{fit}), maximum (σ_{Max}^{Theo}) and minimum (σ_{Min}^{Theo}) theoretically estimated diffusion lengths and final estimated diffusion length.

Bibliography